Dynamic Stability and Levation Control in Maglev Systems

P. Sayegh,* H. Déo,† and Y. Abou Rabii‡
École polytechnique, Institut Polytechnique de Paris, 91120 Palaiseau, France

A. Couairon§
CPHT, CNRS, Ecole polytechnique, Institut Polytechnique de Paris, 91120 Palaiseau, France

This work provides tools for optimizing the stability and levitation of Maglev trains. To optimize passenger capacity, we derive an expression for levitation height as a function of additional weight, refining this model by fitting free parameters to a scaled-down experimental Electromagnetic Suspension (EMS) train. We construct a mathematical model for an Electrodynamic Suspension (EDS) Maglev system, and develop the analytical expressions that describe the system's behavior, ultimately simulating them under standard and extreme conditions. This approach accurately predicts levitation dynamics, with applications toward safer and more efficient Maglev systems and offers groundwork for further stability and load capacity improvements.

I. INTRODUCTION

Magnetic Levitation (Maglev) technology enables contactless suspension and propulsion, offering significant potential to revolutionize transportation by reducing friction and enhancing speed and stability as detailed by Lee *et al.* (2006). However, a major challenge lies in optimizing stability and levitation to improve safety and efficiency under diverse conditions. Maglev systems are broadly classified into Electromagnetic Suspension (EMS), which relies on attractive magnetic forces for levitation, and Electrodynamic Suspension (EDS), which uses repulsive forces induced by currents in conductive guideways.

In this paper, we investigate a simplified EMS system through experimentation and theoretical modeling. By fitting experimental data, we derive an expression for levitation height as a function of mass to optimize the train's capacity. Additionally, we develop a theoretical model of the EDS system to analyze levitation dynamics, including equilibrium height under various conditions. The results demonstrate that the model effectively simulates the system and maintains levitation under extreme scenarios. Together, these contributions advance the understanding of Maglev systems, paving the way for safer and more efficient designs. The code and data used in our simulations can be found on the following repository: https://github.com/peter-sayegh/maglev.git

II. PRINCIPLES OF MAGNETIC LEVITATION

Maglev systems leverage electromagnetic forces to achieve contactless suspension and propulsion. These forces enable frictionless motion, allowing Maglev systems to operate with minimal mechanical wear and reduced energy losses. The fundamental principles governing Maglev systems are rooted in electromagnetic interactions, including force generation, stability, and levitation dynamics.

II.1. General Theory

Maglev systems rely on electromagnetic forces to counteract gravitational forces and achieve stable suspension. The net force on the levitating body can be described as:

$$F_{\text{net}} = F_{\text{mag}} - F_{\text{grav}}, \tag{1}$$

where F_{mag} is the upward magnetic force, and $F_{\text{grav}} = mg$ is the downward gravitational force, with m as the mass of the levitating object and g as the acceleration due to gravity.

For stable levitation, the system must satisfy:

$$F_{\text{mag}} = F_{\text{grav}}, \tag{2}$$

ensuring equilibrium at a specific levitation height. the theorem established by Samuel Earnshaw (1842) states that it is impossible for a static arrangement of charges or magnets to achieve stable equilibrium through purely electrostatic or magnetostatic forces. This implies that additional mechanisms—such as dynamic stabilization or the use of diamagnetic or induced currents—are required to achieve levitation.

Stability depends on the system's ability to restore equilibrium when perturbed. This requires a dynamic variation in the magnetic force, typically achieved through active control (in EMS systems) or passive stabilization (in EDS systems). The condition for stability is quantified by analyzing the vertical force gradient:

$$\frac{\partial F_{\text{mag}}}{\partial z} > 0, \tag{3}$$

where z is the vertical displacement. A positive gradient ensures that an upward displacement reduces the net force, pulling the body back toward equilibrium.

* peter.sayegh@polytechnique.edu
† hadrien.deo@polytechnique.edu
‡ yazan.abou-rabii@polytechnique.edu
§ arnaud.couairon@polytechnique.edu

II.2. Differences Between EMS and EDS

Electromagnetic Suspension (EMS) systems achieve levitation through attractive forces between electromagnets on the vehicle and ferromagnetic materials on the guideway as studied in detail by Jawayant (1973). The electromagnets are actively controlled to maintain stability, as the inherently unstable nature of attractive forces—dictated by Earnshaw's Theorem—requires constant feedback adjustments. EMS systems typically operate with a small levitation gap, on the order of millimeters.

In contrast, Electrodynamic Suspension (EDS) systems rely on repulsive forces generated by induced currents in conductive guideways, as first proposed by Hao *et al.* (2019). The magnetic fields from the train's magnets induce eddy currents in the guideway, creating a repulsive force. This approach circumvents Earnshaw's Theorem by utilizing dynamic magnetic fields and induced currents. EDS systems are passively stable for vertical displacements, as the restoring forces increase with distance. This allows for a larger levitation gap, typically in the range of several centimeters.

While EMS systems require precise active control to counteract instabilities, EDS systems exhibit inherent stability but depend on the vehicle's speed to generate sufficient levitation forces. These differences influence their respective applications and design trade-offs, but both systems share common principles of electromagnetic force generation and stability dynamics.

III. EXPERIMENTAL SETUP

III.1. The Scaled-Down Maglev Train Experiment

A scaled-down Maglev train model was constructed to investigate how the levitation height of the train changes with added mass. The train's base was a wooden block with dimensions of 12 cm (length), 5 cm (width), and 2 cm (height), fitted with Neodymium magnets on its underside. These magnets interacted with magnetic tape laid on the track to achieve levitation. The total mass of the train, including the magnets and wooden block, was $m_0 = 62 \pm 1$ g. The uncertainty in mass measurements is attributed to the precision of the weighing scale used.

The track consisted of a 50 cm strip of magnetic tape attached to a cardboard base, with a width of 8 cm. To maintain lateral stability, 90-degree angle pieces were affixed to the edges of the track, preventing the train from sliding during experimentation. A key component of the setup was the use of monopolar magnetic tape. Therefore, following the approach used in bonded Nd–Fe–B magnet fabrication depicted by Nlebedim *et al.* (2017), where strong external magnetic fields are applied to align internal domains, we repolarized commercially available bipolar magnetic tape by rubbing it with neodymium magnets. This method effectively realigns the tape's magnetic domains to form a monopolar strip as required for stable levitation.

The experimental procedure involved gluing two strips of repolarized magnetic tape onto the underside of the train to form the levitating mechanism. Similarly, two long strips of magnetic tape were affixed to the track to act as rails, with the same monopolar alignment. This configuration ensured stable levitation for the experiment.

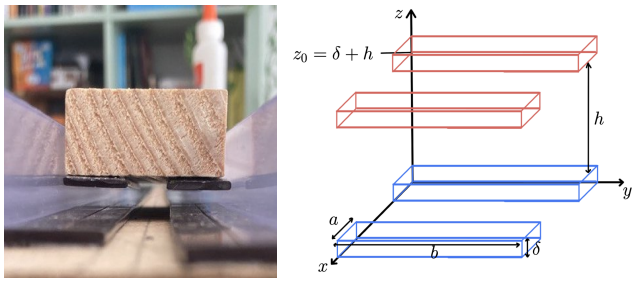

Figure 1. Experimental Maglev Train (left) and Geometry of the experimental setup (right)

III.2. Measurement of Levitation Height

To study the effect of mass on levitation height, a lightweight cardboard cup was placed on top of the train to hold additional weights. Rice was used as an adjustable weight source, allowing precise increments of mass to be added. The mass of the system was measured using a weighing scale with a precision of 1 g, leading to a measurement uncertainty of $u(m) = \pm 1$ g. Levitation height was measured using a ruler with a resolution of 1 mm, and the corresponding uncertainty was taken as $u(h) = \pm 0.5$ mm, accounting for observer error.

The experimental data for levitation height (h) and mass (m) are summarized in Table I (Appendix A). These measurements formed the basis for further theoretical modeling and analysis.

III.3. Force Derivation and Theoretical Fitting

The relationship between the levitation height (h) and added mass (m) was derived by modeling the forces acting on the train. To simplify calculations, we assumed the lower and upper magnets were perfectly aligned, neglecting diagonal forces, and treated the thickness of the magnets as negligible compared to the train's height. The geometry used in this derivation is shown in Fig. 1.

The magnetic force exerted by the guideway on the train in the vertical direction (z) was computed by considering the magnetic dipole interaction. The magnets were modeled as infinitesimal layers of dipoles with a moment $\mathrm{d}\mu = -M\mathrm{d}x\mathrm{d}y\mathrm{d}z\hat{\mathbf{e}}_\mathbf{z}$, where M is the magnetization. The force in the z-direction was derived by integrating

over all lower and upper dipoles:

$$F(z) = \frac{2\mu_0 M^2 \delta}{\pi} \frac{1}{a^2+b^2} \Bigg[z \Bigg(a \sinh^{-1}\left(\frac{a}{z}\right) + b \sinh^{-1}\left(\frac{b}{z}\right) - a \sinh^{-1}\left(\frac{a}{B(z)}\right) - b \sinh^{-1}\left(\frac{b}{A(z)}\right) \Bigg) + ab \left(\tan^{-1}\left(\frac{z}{a}\right) - \tan^{-1}\left(\frac{z}{b}\right) \right) - 2a^2 \tan^{-1}\left(\frac{a(\sqrt{a^2+b^2+z^2} - \sqrt{a^2+b^2})}{z(b+\sqrt{a^2+b^2})} \right) - 2b^2 \tan^{-1}\left(\frac{b(\sqrt{a^2+b^2+z^2} - \sqrt{a^2+b^2})}{z(a+\sqrt{a^2+b^2})} \right) \Bigg]. \tag{4}$$

Here, $A(z) = \sqrt{a^2+z^2}$ and $B(z) = \sqrt{b^2+z^2}$, and a, b, and δ are the rail's width, length, and thickness, respectively. The detailed derivation of the force is given in Appendix B

The equilibrium condition was determined by balancing the magnetic force with the total gravitational force:

$$F(z) = (m + m_0)g. \tag{5}$$

To validate the model, we fitted the experimental data using a linear regression of the form $\hat{m}_i = p\tilde{F}(z_i) + q$, where p and q are fitting parameters. The results are shown in Fig. 2.

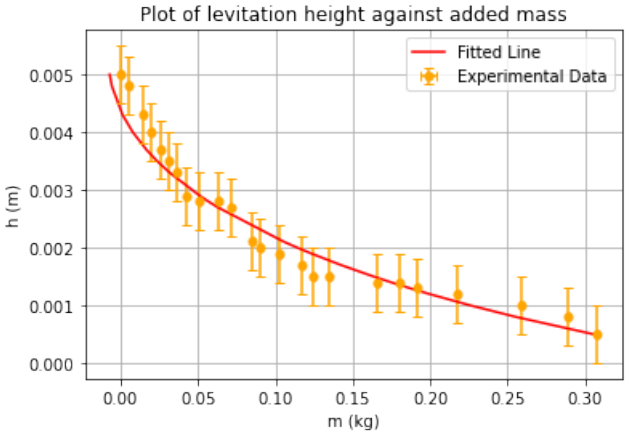

Figure 2. Experimental data and fitted curve $h(m)$

The fitted curve closely matches the experimental data, accurately capturing the non-linear decrease in levitation height with increasing mass. This indicates that the model reflects the underlying physical relationships within the experimental uncertainty.

III.4. Application to a real EMS train

Our experiment and theoretical analysis have culminated in significant findings regarding the electromagnetic suspension (EMS) capabilities of the Maglev system.

As seen in Figure 2 the fit is particularly close to the values between 0.03 and 0.30 kg of added mass. However between 0 and 0.4 the data point seem to decrease in a linear way. In fact, for the three first points, the fit gives a value out of the error bars. Finally, after 0.30 kg, we observe a sharp drop in the train's altitude not modeled by our fit, which continues decreasing until it reaches zero but in a convex manner.

We know from the director of Iran Maglev Technology (IMT) Dr. Hamid Yaghoubi's article in the Journal of Engineering that "In EMS system, the vehicle is levitated about 1 to 2 cm above the guideway using attractive forces" (Yaghoubi 2013). Therefore, we numerically solve $h(m) < h_c = 1cm$ by taking the parameters of a real train i.e. $a = 0.06$m, $b = 153$m, $\delta = 0.0014$m, and $m_0 = 20 \times 10^3$kg.

In this configuration, we obtain a critical mass of 7.5×10^4 kg which corresponds to 941 people with an average mass of 80 kg. This result is close to the maximum capacity of the Shanghai EMS Maglev train, i.e. 959 passengers according to China Discovery (2023), which may serve as a validation of the model when adjusted to reflect practical conditions, confirming that the theoretical predictions can indeed mirror practical outcomes when all relevant factors are considered.

IV. THEORETICAL FRAMEWORK FOR A REAL-WORLD EDS TRAIN

IV.1. Mathematical model of the EDS system

We are interested in constructing a simple mathematical model in order to model the levitation of the Shinkansen L0 series.

In our study, we consider that each side of the train is equipped with a row of identical superconducting coils, all having the same height, shape and size. Adjacent coils carry currents in opposite directions, generating alternating magnetic fields. The guideway consists of a sequence of passive, figure-eight-shaped coils, with no externally applied current.

In addition, since the train and guideway have a plane of symmetry, we will study the system composed of one side of the train and the guideway next to it.

To facilitate analytical solutions we consider the vehicle coils as perfect circles and treat their magnetic field as that of a magnetic dipole. The current in the vehicle coils is assumed to be fixed, neglecting the effect of induction from the guideway coils. The guideway coils, shaped like eights, are modeled as two circular loops with opposing currents, allowing their magnetic fields to be treated as dipoles. From now on, when we refer to a guideway "coil" we refer to the whole eight-shaped coil, while when we refer to a guideway "loop" we only refer to the top or bottom loop which we

use to model the top or bottom part of the whole coil. Further assumptions include considering the magnetic field variation over the guideway as minimal due to distance, neglecting boundary effects due to the train's length and assuming the train moves at a constant speed.

We can now model the system as in Fig. 3.

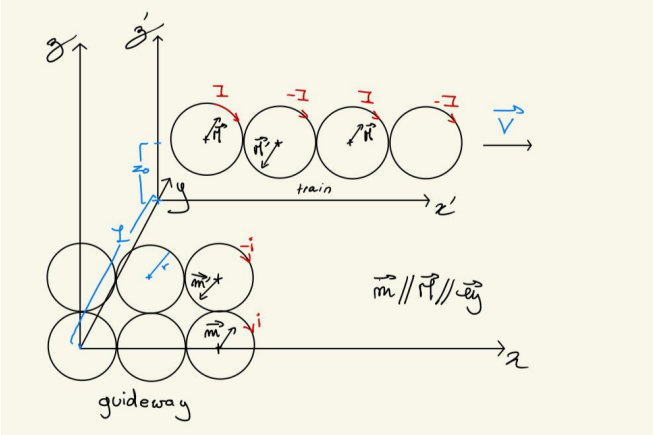

Figure 3. Model for the coils onboard the EDS system and figure of 8 coils on the guideway.

Note that, in the above diagram we have taken multiple conventions which we will keep during the derivation:

- All the currents are taken with the axis of the coil equal to the y-axis, that is with clockwise direction in our diagram.
- The normal to the surface of all the loops is in the $\hat{\mathbf{y}}$ direction.
- The ground is at $z = -r$.

The model, being built specifically for the study of levitation, cannot be used for stability nor propulsion.

IV.2. Energy analysis

To evaluate whether the EDS system can support stable levitation, we analyze the total potential energy of the train as a function of its height. Indeed, cruise speed operation of a maglev train requires an equilibrium between the train's weight and the magnetic levitation force. The latter, generated by the interaction between the guideway's magnetic field and the train's coils, must counteract the gravitational force and maintain stable levitation. Consequently, the vertical equilibrium position of the train must correspond to a minimum in its total potential energy, ensuring that any vertical displacement from this equilibrium position will result in restoring forces that return the train to its original levitated state.

We are therefore looking for the total potential energy of the train as a function of the height of the train, i.e., the sum of the gravitational potential energy and the magnetic potential energy associated with the interaction between the train and the guideway's magnetic fields.

The magnetic energy of the train is the sum of the magnetic energies associated with each of its coils, given by the formula:

$$U_{\text{mag}} = -\sum_{k=1}^{N} \mathbf{M}_k \cdot \mathbf{B}_{\text{guideway}}(\mathbf{r}_k) \tag{6}$$

where $\mathbf{M}_k = (-1)^k I\pi R^2 \hat{\mathbf{y}}$ is the magnetic moment of the k^{th} dipole modeling a coil of the train. The N dipoles form a row of alternate dipoles parallel to the x-axis. The magnetic field $\mathbf{B}_{\text{guideway}}$ is a superposition of all the magnetic fields produced by each guideway coil:

$$\mathbf{B}_{\text{guideway}}(\mathbf{r}_k) = \sum_c \mathbf{B}_c(\mathbf{r}_k) \tag{7}$$

where the magnetic field generated by a guideway's coil writes:

$$\mathbf{B}_c(\mathbf{r}_k) = \frac{\mu_0}{4\pi}\left(\frac{3(\mathbf{m}_c \cdot \mathbf{d}_{ck})\mathbf{d}_{ck}}{d_{ck}^5} - \frac{\mathbf{m}_c}{d_{ck}^3}\right) \tag{8}$$

and $\mathbf{d}_{ck} = \mathbf{r}_k - \mathbf{r}_c$, d_{ck} denotes the distance between the centers of the c-th guideway coil c and the k-th train's coil k.

The magnetic moment of the current loop is given by $\mathbf{m}_c = \pi r^2 i_c \hat{\mathbf{y}}$, with r the radius of the guideway coils, and the current i_c of a guideway coil is given by the following formula:

$$i_c = -\frac{1}{R_e}\frac{d\phi_{c,total}}{dt} \tag{9}$$

where $\phi_{c,total}$ is defined to be the magnetic flux through the surface of the figure-eight shaped guideway coil, and R_e its resistance. For a figure-eight shaped guideway coil, the total flux is the difference between the flux through the bottom and top loop, and each coil in the train contributes to the magnetic flux $\phi_{c,total}$, which can be written as

$$\frac{d\phi_{c,\text{total}}}{dt} = \sum_{k=1}^{N}\left(\frac{d\phi_{ck,\text{bottom}}}{dt} - \frac{d\phi_{ck,\text{top}}}{dt}\right) \tag{10}$$

where the magnetic flux ϕ_{ck} denotes the flux of the magnetic field $\mathbf{B}_k$ generated by the k-th vehicle coil through the c-th guideway loop, see Appendix C:

$$\phi_{ck} = \frac{\mu_0 M_k}{4\pi}\frac{p_{ck}}{\sqrt{r d_{ck}}}\left(K(p_{ck}) + \left(\frac{p_{ck}^2}{2d_{ck}}(d_{ck} - r) - 1\right)\frac{E(p_{ck})}{1 - p_{ck}^2}\right) \tag{11}$$

Here, $K(p)$ and $E(p)$ denote the complete elliptic integrals of the first and second kind, respectively, as defined

in Appendix C. The magnetic flux increases when the train approaches the guideway coil and decreases after it passes it. The magnetic flux therefore depends on time through the projected distance d_{ck} between the coil centers, and the parameter p_{ck}, which both depend on the position $x_k(t)$ of the k-th train coil having the following form:

$$\begin{aligned} x_k &= 2Rk + vt, \\ d_{ck} &= \sqrt{(x_c - x_k)^2 + (z_c - z_0)^2} \\ p_{ck}^2 &= \frac{4rd_{ck}}{L^2 + (d_{ck} + r)^2} \end{aligned} \tag{12}$$

Where L is the distance between the train and the guideway. A closed form formula for the induced current flowing in the c-th guideway coil is given in the Appendix D. We checked that the results obtained by a numerical evaluation of $i_c(t)$ can be reproduced with excellent agreement by discretizing time as $t_n = n\Delta t$, with a step Δt and by calculating

$$i_c(t_n) \simeq \frac{(\phi(t_{n-1}) - \phi(t_{n+1}))}{R_e \Delta t}. \tag{13}$$

From the induced current expressions, we can calculate the magnetic field through equation (8) and subsequently determine the magnetic energy using equation (6). This allows us to construct the total potential energy profile as a function of train height, allowing us to analyze the levitation dynamics and equilibrium positions of the EDS system.

Consequently, the vertical equilibrium position of the train must correspond to a minimum in its total potential energy, ensuring that any vertical displacement from this equilibrium position will result in restoring forces that return the train to its original levitated state. This formulation echoes the findings of Kim *et al.* (1996), who studied the restoring force between two non-coaxial circular coils. They showed that displacing one coil away from alignment with the other creates a spatial variation in mutual inductance, leading to a nonlinear restoring force. While their analysis was based on mutual inductance between two isolated loops, and ours considers a distributed interaction between an array of vehicle coils and figure-eight guideway coils, the core mechanism—stability through minimization of magnetic interaction energy—remains conceptually equivalent.

IV.3. Application to a real EDS train

We want to use the theoretical model constructed in the previous section to study the levitation of the EDS Maglev train. To that end, we use the physical constants reported for the *L0 Shinkansen* series, as documented by Fritz *et al.* (2018). Some parameters, such as the radius of the vehicle and guideway coils, are not publicly specified in detail. We therefore approximate them as $R \approx 0.5\,\mathrm{m}$ and $r \approx 0.25\,\mathrm{m}$, based on figures and schematics from this same reference.

We are first interested in the current's behavior as presented in Fig. 6.

We will present the current in an arbitrary coil of the guideway, intially aligned with the center of the train. Fig. 4 represents the current if one vehicle coil of current I passes by at the speed V of the train.

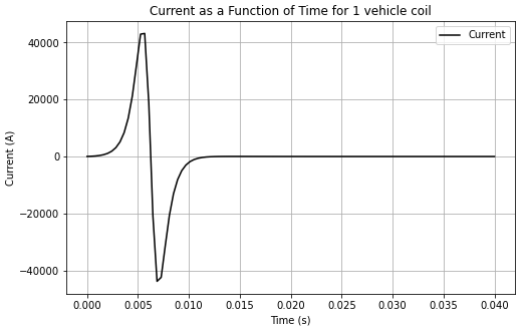

Figure 4. Current for one vehicle coil

The above graph is separated into two parts, one positive and one negative. The positive part corresponds to the interval of time where the vehicle coil (which we will now denote by its current I) approaches the guideway coil (which we will denote by i). Indeed, given that $z_0 > r$ we have that as I approaches, the magnetic flux it creates through the lower loop minus that of the upper loops decreases, so $\frac{d\phi}{dt} < 0$ and thus $i > 0$. The negative part corresponds to I moving away from i, then $\frac{d\phi}{dt} > 0$ and thus $i < 0$.

We now reach an important limitation of our model: During the negative part, and as we considered in the simulation the bottom loop to have normal in the e_y direction, the geometry of our system is shown in Fig. 5 b). Thus the vehicle coil will experience a force upward, creating the levitation. However, for the positive part the geometry is reversed, as shown in Fig. 5 a). Meaning the vehicle coil experiences a force downwards, and thus no levitation.

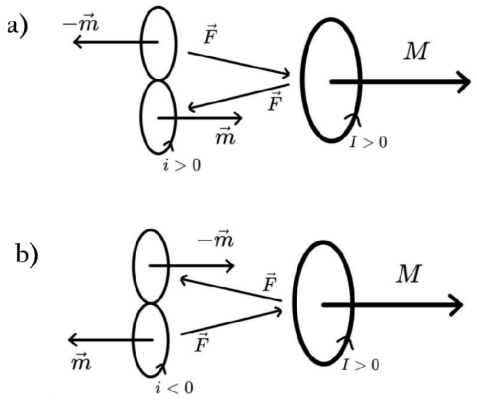

Figure 5. a) Geometry of the system during the positive part of the current curve, the vehicle coil will align with the bottom coil.
b) Geometry of the system during the negative part of the current curve, the vehicle coil will align with the upper coil.

In particular, here the current is symmetric around t such that $i(t) = 0$, meaning that the averaged force on the train is 0, which would induce no levitation.

This argument generalises to a full train of vehicle coil, which yields the current in Fig. 6.

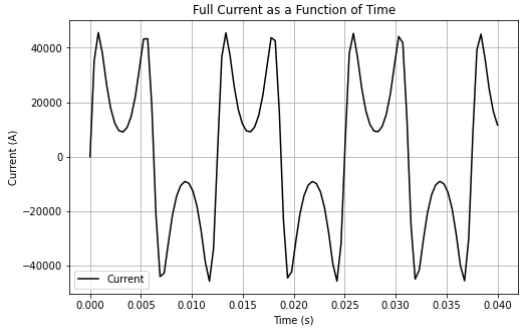

Figure 6. Current for the entire train

This graph is a superposition of many one-coil graphs. In particular, it thus has a periodic profile, with a period of $4R/v$. Indeed, neglecting boundary effects, every $4R/v$ seconds the train has advanced by $4R$ meters and so every vehicle coil with current I has replaced another vehicle coil with current $-I$ and inversly.

In particular this graph reveals the same problem as for the one-coi graph Indeed on the intervals where the current is positive, the geometry of the system will be during the first half that of Fig. 7 a) and during the second half that of Fig. 7 b), thus yielding the same problem as for the one-coil graph.

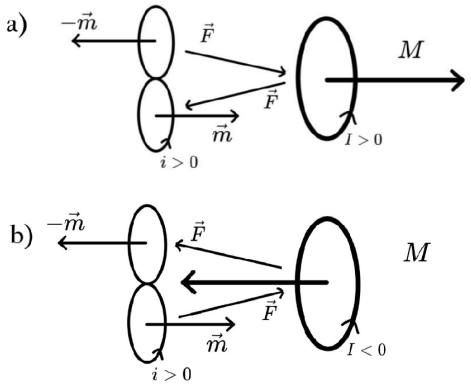

Figure 7. a) Geometry of the system during the first half of the positive part of the current curve, the vehicle coil will align with the bottom coil.
b) Geometry of the system during the second half of the positive part of the current curve, the vehicle coil will align with the upper coil.

Our model thus seem to be incapable to explain levitation. However it gives us insight on two possible behavior of the train which could explain its levitation:

First of all, we have here assumed that train reaches a static equilibrium, i.e. that the train stays at fixed z_0. However, a dynamic equilibrium could also be possible. Indeed, our model reveals that the train could oscillate along the z-axis around a point close to the middle of the guideway coil (where the loops intersect) such that it feels a net upward force over a period. Indeed, by oscillating at the right frequency around this middle, the coil I can consistently create a positive flux, and thus a negative current, yeilding a levitation force as in geometry

FIGURE !!!!!!!!!

, then the train is in dynamic equilibrium. In fact, the periodic nature of the current i would encourage such a dynamic behavior. The time dynamics of the equilibrium will remain out of the scope of this study, we will study specific time point.

Secondly, with greater engineering and an additional energy input one could imagine shifting the period of the current i by a $\frac{\pi}{2}$ phase. Then the bottom loop would always satisfy $i < 0$ and there would thus constantly be an upward force on the train. However, how such a shift can be acheived remains unclear to the authors.

The equilibrium position can then be studied thanks to the energy profile: as detailed above, our program does not capture the time evolution of the system well. Thus we will evaluate at a given time, which we fix to be at $0.45 \times R/v$.

This results in the following energy graph for a train going at $580km/h$, close to its top speed:

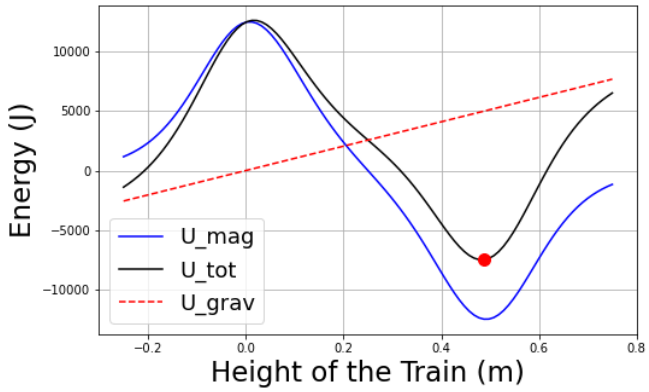

Figure 8. Potential Energy per vehicle coil as a function of the height of the train

Where we find an equilibrium position at $z_0 = 0.49m$, meaning the center of the train's coils are at $r + z_0 = 0.74m$ above ground, since the radius of the coil in the guideway is $0.25m$.

V. RESULTS AND DISCUSSION

V.1. Experimental outcomes

To quantitatively assess the accuracy of our fit in predicting levitation heights based on varying masses, we calculate the coefficient of determination, denoted R^2, which yields an accuracy score of 96.0%. This result is encouraging, yet certain regions reveal limitations in the fit's effectiveness.

However, the high uncertainty in the data, mainly due to the 1 mm uncertainty of the ruler used for measurement, complicates the evaluation of the fit's correspondence with the observed data.

Regarding the accuracy of our fit, we approximated the system by assuming negligible forces between diagonal magnets and considering all four magnets to be identical. Since the experiment itself was an approximation of a maglev train, our fit cannot fully capture the train's behavior, especially under conditions where the assumptions of the system become inadequate—such as when the train is in close proximity to the guideway.

Then as a limitation to our model and fit, we found that the fit diverges from the experimental data in the interval $(0, 0.03)$ kg and for values above 0.30 kg. The linear behavior of the data points under 0.03 kg of added mass can be understood by noting that $m \ll m_0$, so the change in height induced by adding m to the train will result in a change in height $z \ll z_0$. If $H(m)$ is the true function giving the height of the train as a function of m, close to 0 we have

$$H(m) = h_0 + m\frac{dh}{dm},$$

which indicates that the height of the train decreases linearly with the added mass. However, this is not accounted for by our fit, as the function F does not depend on the mass.

Similarly, for masses higher than 0.3 kg, the height decreases sharply. This suggests a maximum in the magnetic force, beyond which the gravitational force prevents the train from levitating. Once again, this behavior is not captured by our fit. Firstly, it was derived under the assumption that the magnets are composed of infinitesimal magnetic dipoles. Two magnetic dipoles create a force that goes to infinity when they get closer. In our case since the dipole are infinitesimal they create a force with finite maximum but which still increases drastically when the magnets are pulled together, thus explaining the convex profile of our fit. Secondly, we assumed that the height of the train is much larger than the thickness of the magnet, which is not true for $m > 0.3kg$.

V.2. Validity of the theoretical EDS model

For what is of the mathematical model we developed, Fig. 8 indicates that levitation occurs approximately at $74cm$ above the ground. Thus, the bottom of the train is more than $R = 50cm$ below the value of z_0. In fact, assuming that there are about 10 to 30 cm of layers of metals under the coil, the underside of the train is 10 cm above the ground. This is indeed how the Shinkansen behaves in real life. However, some constants of the L0 series are not directly available in open sources and were thus estimated.

However, it is important to note two major limitations of our mathematical model.

Firstly, our model does not appropriately represent the time evolution of the system. As shown before, for a given time (here $t = 0.4 \times R/v$) our model represents well the levitation of the train. However, if we let the system evolve further, one will observe unexpected behaviors. Most notably, the magnetic energy graph will inverse, leaving no more room for levitation, as shown in Fig. 9 for $t = 0.6 \times R/v$:

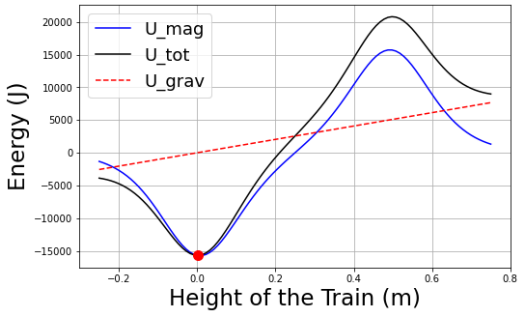

Figure 9. Potential energy under standard conditions at t = $0.6 \times R/v$s

This is because of the simplicity of our model and was partly discussed during the discussion about the current's profile. Indeed, our system does not encompass all of the dynamics, most notably it does not take into consideration the induction effect of guideway coils on vehicle coils, which have an impact on time evolution. Similarly, the system only considers one row of vehicle coil and the associated part of the guideway, therefore neglecting the impact of the symmetric part: the opposite row of vehicle coils and its guideway. All in all this results in a model which is too simplified to correctly account for time evolution.

Secondly, when simulating the behavior of the system at very high speed we found:

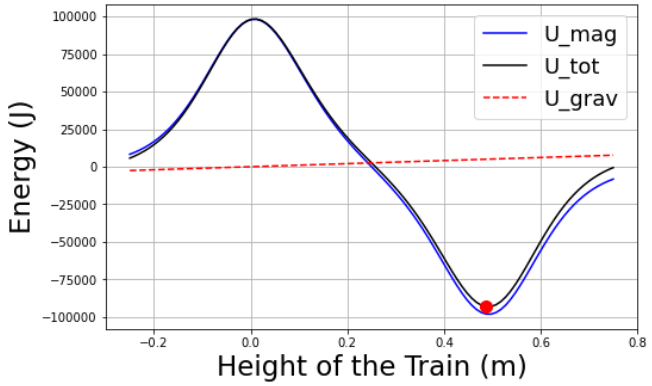

Figure 10. Potential energy for v = 1000 m.s^{-1}

This is not what is expected. The maglev train should not be able to go over 650 km.h^{-1} despite our results showing a stable equilibrium point in Fig. 10. This inconsistency is due to the limitations of our system. Indeed, our model does not take into consideration the mechanisms associated with propulsion.

Indeed, we considered that the magnetic field used for propulsion does not impact the levitation. This was justified as this magnetic field should create a force in the $\hat{e}_x$ direction, thus not impacting the $\hat{e}_y$ direction. However, at speeds over 650 km.h^{-1}, this magnetic field is extremely large, hence its $\hat{e}_y$ component is not negligible anymore. it could be responsible for a loss of levitation, or stability, preventing the train from accelerating above 650 km.h^{-1}.

It is also possible that the propulsion mechanisms do not have the capacity to propel the train at such a speed. Then the error would be that we assumed that reaching such a speed was possible.

AUTHOR DECLARATIONS

The authors have no conflicts to disclose.

H.-W. Lee, K.-C. Kim, and J. Lee, IEEE Transactions on Magnetics **42**, 1917 (2006).

S. Earnshaw, Transactions of the Cambridge Philosophical Society **7**, 97 (1842).

B. Jawayant, Rep. Prog. Phys. **44**, 411 (1973).

L. Hao, Z. Huang, F. Dong, D. Qiu, B. Shen, and Z. Jin, IEEE Transactions on Applied Superconductivity 10.1109/TASC.2018.2881688.

I. C. Nlebedim, H. Ucar, C. B. Hatter, R. W. McCallum, M. P. Paranthaman, M. S. Kesler, J. Ormerod, and et al., Journal of Magnetism and Magnetic Materials **422**, 168 (2017).

H. Yaghoubi, Journal of Engineering **2013**, Article ID 537986, 19 pages (2013).

China Discovery, "Shanghai maglev train," `https://www.chinadiscovery.com/shanghai/shanghai-maglev.html` (2023).

K. Kim, E. Levi, Z. Zabar, and L. Birenbaum, IEEE Transactions on Magnetics **32**, 478 (1996).

E. Fritz, L. Blow, J. Kluhspies, R. Kircher, and M.-H. Witt, Transportation Systems and Technology , 134.

M. Abramowitz and I. A. Stegun, *Handbook of Mathematical Functions with Formulas, Graphs, and Mathematical Tables* (Dover Publications, New York, 1964).

Appendix A: Experimental Data

Table I. Experimental data for the mass (m) and levitation height (h) of the Maglev train model. The uncertainties are ± 1 g for m and ± 0.5 mm for h.

m (g)	0	5	15	20	26	31	36	43	51	63
h (mm)	5.0	4.8	4.3	4.0	3.7	3.5	3.3	2.9	2.8	2.8
m (g)	71	85	90	103	117	124	135	166	180	192
h (mm)	2.7	2.1	2.0	1.9	1.7	1.5	1.5	1.4	1.4	1.3
m (g)	217	259	289	307	322					
h (mm)	1.2	1.0	0.8	0.5	0.0					

Appendix B: Analytical Derivation of the Force Induced by the Dipole Moment

In this section, we derive the expression for the magnetic force $F(z)$ acting on a Maglev train system, modeled as layers of magnetic dipoles.

We model each rail as a continuous surface distribution of magnetic dipoles. Let M be the surface magnetization

of the rail, oriented along the z-axis. The infinitesimal dipole moment of an element of the rail is defined as:

$$d\boldsymbol{\mu} = M\, dx'\, dy'\, \hat{\mathbf{z}},$$

The objective is to calculate the magnetic force between two layers of dipoles (representing the upper and lower rails) as a function of the distance z between them.

The magnetic vector potential $\mathbf{A}$ at a point $\mathbf{r} = (x, y, z)$ due to an infinitesimal surface dipole element located at $\mathbf{r}' = (x', y', 0)$ is given by:

$$d\mathbf{A}(\mathbf{r}) = \frac{\mu_0 M}{4\pi} \frac{d\boldsymbol{\mu} \times (\mathbf{r} - \mathbf{r}')}{|\mathbf{r} - \mathbf{r}'|^3}$$

$$d\mathbf{A}(\mathbf{r}) = \frac{\mu_0 M}{4\pi} \frac{dx'dy'}{[(x-x')^2 + (y-y')^2 + z^2]^{3/2}} \begin{bmatrix} -(y-y') \\ x - x' \\ 0 \end{bmatrix},$$

where μ_0 is the permeability of free space ($\mu_0 = 4\pi \times 10^{-7}\,\mathrm{N/A}^2$).

To find the total vector potential generated by the lower rail of width a and length b, we integrate over the entire surface of the bottom rail:

$$\mathbf{A}(\mathbf{r}) = \frac{\mu_0 M}{4\pi} \int_{x-a}^{x} \int_{y-b}^{y} \frac{dXdY}{[X^2 + Y^2 + z^2]^{3/2}} \begin{bmatrix} -Y \\ X \\ 0 \end{bmatrix}.$$

where we did the change of variable $X = x - x', Y = y - y'$.

We derive the integrals necessary to calculate the magnetic potential and force in the system. The integrals will be evaluated over the specified ranges using the correct variables dX and dY.

$$I_0(X) = \int_{y-b}^{y} \frac{Y dY}{(X^2 + Y^2 + z^2)^{3/2}}) = \left[\frac{1}{\sqrt{X^2 + Y^2 + z^2}} \right]_{Y=y-b}^{y}$$

$$I_1(Y) = \int_{x-a}^{x} \frac{X dX}{(X^2 + Y^2 + z^2)^{3/2}}. = \left[\frac{1}{\sqrt{X^2 + Y^2 + z^2}} \right]_{X=x-a}^{x}.$$

$$I_2 = \int_{x-a}^{x} I_0(X) dX = \left[\ln \left(\frac{\sqrt{X^2 + y^2 + z^2} + X}{\sqrt{X^2 + (y-b)^2 + z^2} + X} \right) \right]_{X=x-a}^{x}.$$

$$I_3 = \int_{y-b}^{y} I_1(Y) dY = \left[\ln \left(\frac{\sqrt{(x-a)^2 + Y^2 + z^2} + Y}{\sqrt{x^2 + Y^2 + z^2} + Y} \right) \right]_{Y=y-b}^{y}.$$

From there, one gets the full expression of the vector potential $\mathbf{A}(\mathbf{r})$:

$\mathbf{A}(\mathbf{r}) =$

$$\frac{\mu_0 M}{4\pi} \begin{pmatrix} \ln \left(\frac{\sqrt{(y-b)^2+z^2+(x-a)^2}+(x-a)}{\sqrt{(y-b)^2+z^2+x^2}+x} \frac{\sqrt{y^2+z^2+x^2}+x}{\sqrt{y^2+z^2+(x-a)^2}+(x-a)} \right) \\ \ln \left(\frac{\sqrt{(y-b)^2+z^2+x^2}+(y-b)}{\sqrt{y^2+z^2+x^2}+y} \frac{\sqrt{y^2+z^2+(x-a)^2}+y}{\sqrt{(y-b)^2+z^2+(x-a)^2}+(y-b)} \right) \\ C \end{pmatrix}.$$

The magnetic field $\mathbf{B}$ can be derived from the vector potential $\mathbf{A}$ using the relation:

$$\mathbf{B} = \nabla \times \mathbf{A}.$$

However, due to the symmetry of the system, only the z-component of the magnetic field is significant for our analysis. Thus, we focus on calculating B_z, which is given by:

$$B_z = \frac{\partial A_y}{\partial x} - \frac{\partial A_x}{\partial y}.$$

The upper rail, placed at a height z, consists of a layer of dipole moments aligned downward:

$$d\boldsymbol{\mu} = -M\, dx\, dy\, \hat{\mathbf{z}}.$$

The force on each dipole in the presence of a magnetic field is given by:

$$d\mathbf{F} = \nabla(d\boldsymbol{\mu} \cdot \mathbf{B}).$$

To find the total force on both upper rails by both lower rails, we integrate over its surface. The z-component of the force is:

$$F(z) = -2M \int_0^a \int_0^b \partial_z B_z(z) dx dy.$$

$$F(z) = -2M \int_0^a dx \int_0^b \partial_z(\partial_x A_y - \partial_y A_x) dy.$$

$$F(z) = -2M \frac{\partial}{\partial z} \left(\int_0^b [A_y]_{x=0}^{a} dy - \int_0^a [A_x]_{y=0}^{b} dx \right).$$

Using the identities:

$$\sinh^{-1}(U) = \ln(\sqrt{1 + U^2} + U)$$

and

$$\int_0^{U_m} \sinh^{-1}(\frac{U}{U_0}) dU = U_m \sinh^{-1}(\frac{U_m}{U_0}) - \sqrt{U_0^2 + U_m^2} + U_0$$

we obtain the following expression of the induced force along the z-axis:

$$F(z) = -\frac{2\mu_0 M^2}{\pi} \frac{\partial \Phi}{\partial z}(z)$$

where Φ, defined below, is a dimensionless potential for the force:

$$\Phi(z) = a \sinh^{-1}\left(\frac{a}{z}\right) + b \sinh^{-1}\left(\frac{b}{z}\right) - a \sinh^{-1}\left(\frac{a}{B(z)}\right) - b \sinh^{-1}\left(\frac{b}{A(z)}\right) - 2(A(z) + B(z)) + 2(z + \sqrt{a^2 + b^2 + z^2}) \tag{B1}$$

With $A(z) = \sqrt{a^2 + z^2}$ and $B(z) = \sqrt{b^2 + z^2}$

To extend our results to a more realistic 3D scenario, we consider the finite thickness δ of the upper rail. The magnetic field correction can be approximated as:

$$F^{(3D)}(z) \propto \frac{\partial B_z^{(3D)}}{\partial z} \approx B_z^{(2D)}(z+\delta) - B_z^{(2D)}(z).$$

This approximation accounts for the finite thickness of the magnetic layers and provides a more accurate representation of the force. We proceed as follows:

First, we consider an elementary dipole moment $d\boldsymbol{\mu} = -M_{3D}dxdydz\hat{\mathbf{z}}$ where $M_{3D} = \frac{M_{2D}}{\delta}$ is the magnetization in A/m, which can be defined as the density of dipole moments per unit volume.

$$\mathbf{F} = 2\int_0^a \int_0^b \int_{z_0}^{z_0+\delta} \nabla(d\boldsymbol{\mu}\cdot\mathbf{B}).$$

Since we are only interested in F_z by symmetry, we proceed as follows:

$$F_z(z) = -2M_{3D}\int_0^a \int_0^b \int_{z_0}^{z_0+\delta} B_z^{3D}(z)\; dx\, dy\, dz.$$

Expanding further, using the above approximation:

$$F_z = -2M_{3D}\int_{z_0}^{z_0+\delta} \int_0^b \int_0^a \left(\frac{\partial}{\partial z}\int_0^\delta B_z^{2D}(z-z')\, dz'\right) dxdydz.$$

$$F_z = \frac{1}{\delta}\int_{z_0}^{z_0+\delta} dz \int_z^{z-\delta} dz' \left(\int_0^a \int_0^b -2M\partial_z B_z^{(2D)}(z)\, dx\, dy\right).$$

On the other hand, we recognize the force expression we had using the zero-thickness model (i.e. in two dimensions):

$$F_z^{(2D)} = -2\int_0^b \int_0^a M_{2D}\, dx\, dy\, \partial_z B_z^{(2D)}(z).$$

Thus:

$$F_z = \frac{1}{\delta}\int_{z_0}^{z_0+\delta} dz \int_{z-\delta}^{z} \left[F_z^{(2D)}(z')\right] dz'.$$

$$F_z = -\frac{2\mu_0 M_{3D}^2\delta}{\pi}\int_{z_0}^{z_0+\delta} dz \int_{z-\delta}^{z} \left[\frac{\partial\Phi}{\partial z}(z')\right] dz'.$$

Given a position z_0 below the top rail, we have:

$$F_z(z_0) = -\frac{2\mu_0 M_{3D}^2\delta}{\pi}\int_{z_0}^{z_0+\delta} (\Phi(z-\delta) - \Phi(z))\, dz$$

We define the primitive Ψ of Φ:

$$\Psi(z) = \int \Phi(z)\, dz.$$

Step-by-Step Derivation:

$$J_0 = \int a\, \sinh^{-1}(\frac{a}{z})\, dz.$$

$$J_0 = a\, z\, \sinh^{-1}(\frac{a}{z}) + a^2 \ln\left(z + \sqrt{a^2+z^2}\right).$$

$$J_1 = \int b\, \sinh^{-1}(\frac{b}{z})\, dz.$$

$$J_1 = b\, z\, \sinh^{-1}(\frac{b}{z}) + b^2 \ln\left(z + \sqrt{b^2+z^2}\right).$$

$$J_2 = \int -a\, \sinh^{-1}(\frac{a}{B(z)})\, dz.$$

$$J_2 = -a\, z\, \sinh^{-1}(\frac{a}{B(z)}) + 2a^2 \arctan\left(\frac{z}{\sqrt{a^2+b^2}}\right).$$

$$J_3 = \int -b\, \sinh^{-1}(\frac{b}{A(z)})\, dz.$$

$$J_3 = -b\, z\, \sinh^{-1}(\frac{b}{A(z)}) + 2b^2 \arctan\left(\frac{z}{\sqrt{a^2+b^2}}\right).$$

$$J_4 = \int -2\big(A(z) + B(z)\big)\, dz$$

$$\begin{aligned} J_4 = &-\left[z\sqrt{a^2+z^2} + a^2 \sinh^{-1}\left(\frac{z}{a}\right)\right] \\ &-\left[z\sqrt{b^2+z^2} + b^2 \sinh^{-1}\left(\frac{z}{b}\right)\right]. \end{aligned} \quad \text{(B2)}$$

$$J_5 = \int 2\left(z + \sqrt{a^2+b^2+z^2}\right)\, dz$$

$$J_5 = z^2 + z\sqrt{a^2+b^2+z^2} + (a^2+b^2)\sinh^{-1}\left(\frac{z}{\sqrt{a^2+b^2}}\right).$$

So, by combining all terms, the final expression for $\Psi(z)$ is:

$$\begin{aligned} \Psi(z) = &\, a\, z\, \sinh^{-1}(\frac{a}{z}) + b\, z\, \sinh^{-1}(\frac{b}{z}) \\ &- a\, z\, \sinh^{-1}(\frac{a}{B(z)}) - b\, z\, \sinh^{-1}(\frac{b}{A(z)}) \\ &- z\sqrt{a^2+z^2} - a^2 \sinh^{-1}\left(\frac{z}{a}\right) \\ &- z\sqrt{b^2+z^2} - b^2 \sinh^{-1}\left(\frac{z}{b}\right) \\ &+ z^2 + z\sqrt{a^2+b^2+z^2} + (a^2+b^2)\sinh^{-1}\left(\frac{z}{\sqrt{a^2+b^2}}\right). \end{aligned} \quad \text{(B3)}$$

Hence, we obtain an expression of F_z the force induced by the magnetic dipole moment on the top rails along the z-axis:

$$F_z(z_0) = \frac{2\mu_0 M_{3D}^2\delta}{\pi(a^2+b^2)}(\Psi(z_0+\delta) + \Psi(z_0-\delta) - 2\Psi(z_0))$$

Then, we generalize to an arbitrary position z between the two rails, drop the 2D/3D indices, consider $\delta/z << 1$ and find:

$$F(z) = \frac{2\mu_0 M^2 \delta}{\pi} \frac{1}{a^2+b^2} \Bigg[z \Bigg(a \sinh^{-1}\left(\frac{a}{z}\right) + b \sinh^{-1}\left(\frac{b}{z}\right) - a \sinh^{-1}\left(\frac{a}{B(z)}\right) - b \sinh^{-1}\left(\frac{b}{A(z)}\right) \Bigg) + ab \left(\tan^{-1}\left(\frac{z}{a}\right) - \tan^{-1}\left(\frac{z}{b}\right) \right) - 2a^2 \tan^{-1}\left(\frac{a(\sqrt{a^2+b^2+z^2} - \sqrt{a^2+b^2})}{z(b+\sqrt{a^2+b^2})} \right) - 2b^2 \tan^{-1}\left(\frac{b(\sqrt{a^2+b^2+z^2} - \sqrt{a^2+b^2})}{z(a+\sqrt{a^2+b^2})} \right) \Bigg]. \quad \text{(B4)}$$

Appendix C: Derivation of the magnetic flux by one vehicle coil through one guideway loop

We consider a system where vehicle coils, described as N magnetic dipole moments $\mathbf{M}_k$, interact with guideway loops, as shown in Fig. 3. The position of the k^{th} train's coil is $(x_k, y_k, z_k) = (2Rk + vt, L, z_0)$, and thus the position of a point $\mathbf{r}$ on the guideway with respect to the position of the center of the k^{th} train's coil is

$$\mathbf{r} - \mathbf{r_k} = \begin{pmatrix} x - x_k \\ -L \\ z - z_0 \end{pmatrix} \quad \text{(C1)}$$

where L is the gap between the train and the guideway wall, and z_0 is the equilibrium height of the train.

The magnetic dipole moment M_k alternates direction for adjacent coils and is given by:

$$\mathbf{M}_k = M_k \hat{\mathbf{y}} = (-1)^k M \hat{\mathbf{y}} \quad \text{(C2)}$$

where $M = \pi R^2 I$, with R being the radius of the vehicle coil and I the current. This alternating pattern ensures opposite current directions in adjacent coils. Furthermore, we can now express the magnetic field generated by dipole moment $\mathbf{M}_k$ at position $\mathbf{r}$, using the magnetic vector potential of a coil:

$$\mathbf{B}_k(\mathbf{r}) = \boldsymbol{\nabla} \times \mathbf{A}_k \quad \text{with} \quad \mathbf{A_k}(\mathbf{r}) = \frac{\mu_0}{4\pi} \frac{\mathbf{M}_k \times (\mathbf{r} - \mathbf{r}_k)}{|\mathbf{r} - \mathbf{r}_k|^3} \quad \text{(C3)}$$

Owing to Stokes's theorem, the magnetic flux through a surface S bordered by loop C is given by the circulation of the vector potential along the contour C:

$$\phi_k = \iint_S \mathbf{B}_k(\mathbf{r}) \cdot \hat{\mathbf{y}} \, dS = \oint_C \mathbf{A_k}(\mathbf{r}) \cdot d\mathbf{r} \quad \text{(C4)}$$

The closed loop C represents a coil of the guideway. It is a circle centered at $\mathbf{r}_c = (x_c, 0, z_c)$. To calculate the line integral of the magnetic vector potential around C, we use a polar coordinate system $(\hat{\boldsymbol{\rho}}, \hat{\boldsymbol{\theta}})$ centered at $\mathbf{r}_c$ in the xz-plane, expressing the coordinates of a point on the loop as

$$\mathbf{r} = \mathbf{r}_c + r(\cos\theta \, \hat{\mathbf{x}} + \sin\theta \, \hat{\mathbf{z}}). \quad \text{(C5)}$$

Defining $\mathbf{d} = \mathbf{r}_c - \mathbf{r}_k + L\hat{\mathbf{y}}$, we can express the position of a point on contour C relative to the center of a train's coil as

$$\mathbf{r} - \mathbf{r}_k = \mathbf{d} - L\hat{\mathbf{y}} + r\hat{\boldsymbol{\rho}} \quad \text{(C6)}$$

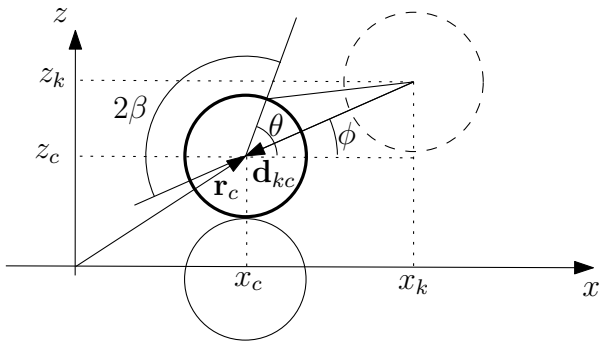

Figure 11.

and the squared distance as

$$|\mathbf{r} - \mathbf{r}_k|^2 = d^2 + L^2 + r^2 + 2r\mathbf{d} \cdot \hat{\boldsymbol{\rho}} \quad \text{(C7)}$$

where $d = \sqrt{(x_c - x_k)^2 + (z_c - z_0)^2}$. Writing $\mathbf{d} = -d(\cos\phi \, \hat{\mathbf{x}} + \sin\phi \, \hat{\mathbf{z}})$, and defining $\beta = (\theta - \phi)/2$, we have:

$$\begin{aligned} |\mathbf{r} - \mathbf{r}_k|^2 &= L^2 + (d+r)^2 - 4rd\sin^2\beta \\ &= \frac{4rd}{p^2}(1 - p^2\sin^2\beta) \end{aligned} \quad \text{(C8)}$$

where p denotes a number smaller than one defined as

$$p^2 = \frac{4rd}{L^2 + (d+r)^2}. \quad \text{(C9)}$$

Furthermore, we can express the infinitesimal length in polar coordinates, $d\mathbf{r} = rd\theta(-\sin\theta \, \hat{\mathbf{x}} + \cos\theta \, \hat{\mathbf{z}})$, allowing us to express the scalar product $\mathbf{A_k} \cdot d\mathbf{r}$:

$$\begin{aligned} \mathbf{A_k} \cdot d\mathbf{r} &= \frac{\mu_0 M_k}{4\pi |\mathbf{r} - \mathbf{r}_k|^3} \begin{pmatrix} (z_c - z_0) + r\sin\theta \\ 0 \\ -(x_c - x_k) - r\cos\theta \end{pmatrix} \cdot rd\theta \begin{pmatrix} -\sin\theta \\ 0 \\ \cos\theta \end{pmatrix} \\ &= \frac{\mu_0 M_k}{4\pi |\mathbf{r} - \mathbf{r}_k|^3} rd\theta(d - r - 2d\sin^2\beta) \end{aligned} \quad \text{(C10)}$$

Note that $d\theta = 2d\beta$, allowing us to write the expression of the flux as the integral of an even function of β, for $0 \leq \beta \leq \pi/2$:

$$\phi_k = \frac{\mu_0 M_k r}{\pi} \left(\frac{p^2}{4rd}\right)^{3/2} \int_0^{\pi/2} \frac{(d-r) - 2d\sin^2\beta}{(1 - p^2\sin^2\beta)^{3/2}} d\beta. \quad \text{(C11)}$$

We can rewrite the numerator inside the integral as:

$$d - r - 2d\sin^2\beta = \frac{2d}{p^2}(1 - p^2\sin^2\beta) + d - r - \frac{2d}{p^2} \quad \text{(C12)}$$

Leading to,

$$\phi_k = \frac{\mu_0 M_k}{4\pi} \frac{p}{\sqrt{rd}} \left(K(p) + \left(\frac{p^2}{2}\left(1 - \frac{r}{d}\right) - 1 \right) \frac{E(p)}{1 - p^2} \right) \quad \text{(C13)}$$

where $K(p)$ and $E(p)$ denote the complete elliptic integrals of the first and second kind (Abramowitz and Stegun 1964), respectively:

$$\begin{aligned} K(p) &= \int_0^{\pi/2} \frac{d\theta}{\sqrt{1-p^2\sin^2\theta}} \\ E(p) &= \int_0^{\pi/2} \sqrt{1-p^2\sin^2\theta}\, d\theta. \end{aligned} \tag{C14}$$

The flux Φ_k of the k-th dipole moment in the train through the guideway loop centered at $\mathbf{r}_c$ depends on both $\mathbf{r}_k$ and $\mathbf{r}_c$ via the distance d and parameter p.

Appendix D: Derivation of the induced current in a figure-eight shaped guideway coil

The magnetic flux ϕ_{ck} through the c-th guideway loop due to the k-th vehicle coil is given by equation (11). To find the induced current according to Faraday's law, we need to calculate the time derivative $\frac{d\phi_{ck}}{dt}$.

From equation (11), the flux expression can be decomposed as $\phi_{ck} = A \cdot B(C + D)$ where the components are defined as:

$$\begin{aligned} A &= \frac{\mu_0 M_k}{4\pi} \\ B &= \frac{p_{ck}}{\sqrt{r d_{ck}^3}} \\ C &= -\frac{(2d_{ck} + p_{ck}^2(r - d_{ck}))E(p_{ck})}{1 - p_{ck}^2} \\ D &= 2d_{ck}K(p_{ck}) \end{aligned} \tag{D1}$$

The time derivative of the flux becomes:

$$\frac{d\phi_{ck}}{dt} = A\left(\dot{B}(C + D) + B(\dot{C} + \dot{D})\right) \tag{D2}$$

In order to evaluate this expression, we derive each component systematically. The derivative of component B is:

$$\dot{B} = \frac{d}{dt}\left(\frac{p_{ck}}{\sqrt{r d_{ck}^3}}\right) = \frac{\dot{p}_{ck}\sqrt{r d_{ck}^3} - \frac{3p_{ck} r \dot{d}_{ck} d_{ck}^2}{2\sqrt{r d_{ck}^3}}}{r d_{ck}^3} \tag{D3}$$

For component C, we obtain:

$$\dot{C} = -\frac{(2\dot{d}_{ck} + 2\dot{p}_{ck}p_{ck}(r - d_{ck}) - \dot{d}_{ck}p_{ck}^2)E(p_{ck})}{1 - p_{ck}^2} \tag{D4}$$

$$- \frac{\left((1 - p_{ck}^2)\dot{E}(p_{ck}) + 2p_{ck}\dot{p}_{ck}E(p_{ck})\right)(2d_{ck} + p_{ck}^2(r - d_{ck}))}{(1 - p_{ck}^2)^2} \tag{D5}$$

Similarly, the derivative of component D is:

$$\dot{D} = \frac{\left(2\dot{d}_{ck}K(p_{ck}) + 2d_{ck}\dot{K}(p_{ck})\right)p_{ck}^2 - 2d_{ck}K(p_{ck})(2p_{ck}\dot{p}_{ck})}{p_{ck}^4} \tag{D6}$$

Furthermore, from the original expression of $x_k = 2Rk + vt$, $d_{ck} = \sqrt{(x_c - x_k)^2 + (z_c - z_0)^2}$, and $p_{ck}^2 = \frac{4rd_{ck}}{L^2 + (d_{ck} + r)^2}$. The corresponding time derivatives are:

$$\dot{d}_{ck} = \frac{v(x_k - x_c)}{d_{ck}} \tag{D7}$$

$$\dot{p}_{ck} = \frac{\dot{d}_{ck}}{2d_{ck}} p_{ck}\left(1 - \left(1 + \frac{d_{ck}}{r}\right)\frac{p_{ck}^2}{2}\right) \tag{D8}$$

The time derivatives of the complete elliptic integrals are given by standard identities:

$$\frac{dE(p_{ck}(t))}{dt} = \frac{\dot{p}_{ck}}{p_{ck}}(E(p_{ck}) - K(p_{ck})) \tag{D9}$$

$$\frac{dK(p_{ck}(t))}{dt} = \frac{\dot{p}_{ck}}{p_{ck}}\left(\frac{E(p_{ck})}{1 - p_{ck}^2} - K(p_{ck})\right) \tag{D10}$$

For a figure-eight shaped guideway coil, the total flux is the difference between the flux through the bottom and top loops: $\phi_{c,\text{total}} = \sum_{k=1}^{N}(\phi_{ck,\text{bottom}} - \phi_{ck,\text{top}})$. The time derivative of this total flux is:

$$\frac{d\phi_{c,\text{total}}}{dt} = \sum_{k=1}^{N}\left(\frac{d\phi_{ck,\text{bottom}}}{dt} - \frac{d\phi_{ck,\text{top}}}{dt}\right) \tag{D11}$$

According to Faraday's law, the induced current in the c-th guideway coil is $i_c = -\frac{1}{R_e}\frac{d\phi_{c,\text{total}}}{dt}$, where R_e is the resistance of the guideway coil.